

RECENT RESULTS FROM THE PHENIX EXPERIMENT AT RHIC*

SENTA VICTORIA GREENE

for the PHENIX Collaboration

Vanderbilt University
Box 1807-B, Nashville, TN 37235, USA

(Received May 20, 2002)

Selected data from the first two running periods of the PHENIX detector at the Relativistic Heavy Ion Collider are presented and discussed. These results emphasize charged particle multiplicity as a function of centrality, suppression of hadron production at high transverse momentum, and an estimate of open charm production from single electron spectra.

PACS numbers: 25.75.Dw

1. Introduction

A major goal of the PHENIX experiment is to detect and study the physical properties of the quark–gluon plasma. The design of the PHENIX experiment was driven by the goal of building a detector that would allow the measurement of many different signals from heavy-ion collisions at RHIC. By keeping the scope of the measurements broad, it is expected that all stages of the collision process, from the early stages to subsequent hadronization, can be studied. The PHENIX detector can measure hadrons, leptons, and photons with excellent momentum and energy resolution. The PHENIX design also has enough versatility to be used to study proton spin using the polarized proton beams at RHIC, although that physics program is outside the scope of this paper.

The final detector design (Fig. 1) comprises a central spectrometer which measures hadrons, electrons, and photons at midrapidity and two muon spectrometer arms which are sensitive to muons at forward rapidities. The two arms of the central spectrometer arms each cover 90 degrees in azimuth with

* Presented at the Cracow Epiphany Conference on Quarks and Gluons in Extreme Conditions, Cracow, Poland, January 3–6, 2002.

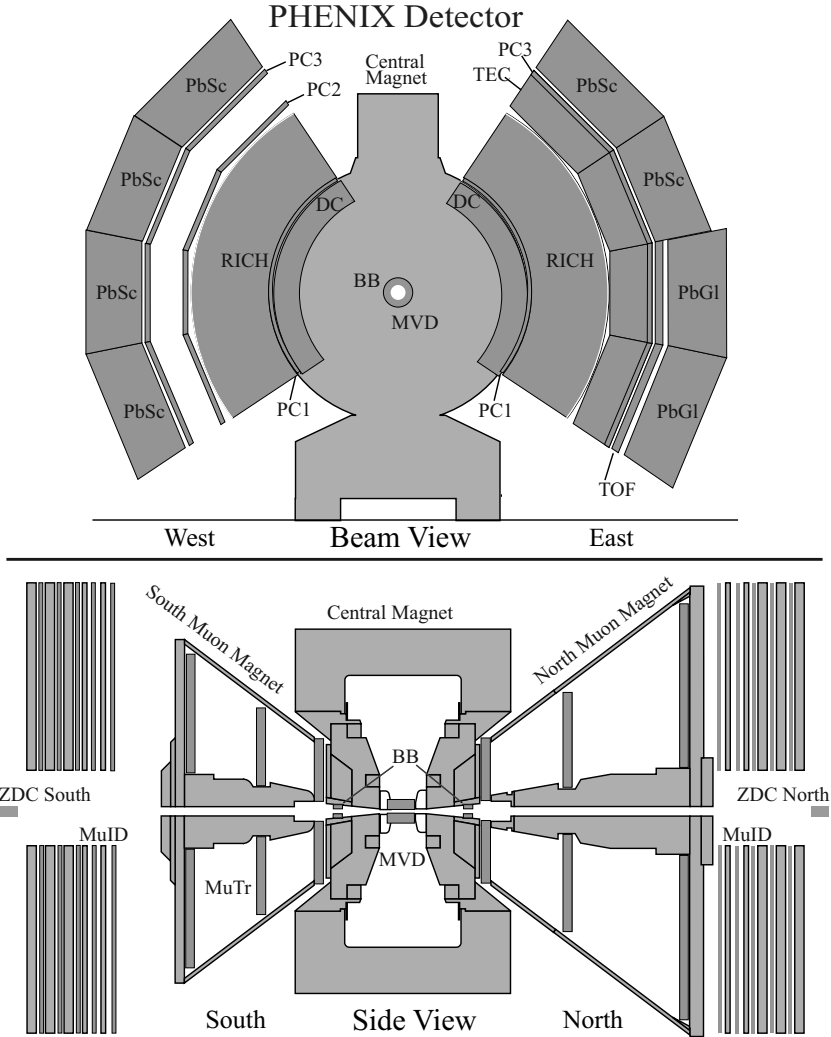


Fig. 1. The complete PHENIX detector as designed. The specific configuration of the detector depends on the year in which the data were taken.

$|\eta| < 0.35$. Each muon arm has full azimuthal coverage and $1.1 < |\eta| < 2.4$. The central arms have three tracking systems, Pad Chambers (PC), Drift Chambers (DC), and Time-Expansion Chambers (TEC). For particle identification there are a Ring-Imaging Cerenkov (RICH) counter and a Time-Of-Flight hodoscope (TOF). Energy measurements are made using two types of ElectroMagnetic CALorimeters (EMCAL), lead-glass (PbGl) and lead-scintillator (PbSc). The muon arms have tracking consisting of three stations of cathode strip chambers (MuTr) and particle identification from five layers

of Iarocci tubes with iron absorber (MuID). In addition to the spectrometer arms, there are three detectors which can be used for event characterization and measurement of global properties: A quartz Cerenkov Beam-Beam Counter (BBC) [2], the standard RHIC Zero-Degree Calorimeter (ZDC) [3], and a silicon-strip Multiplicity and Vertex Detector (MVD). Some parts of the detector were either not installed or not instrumented during one or both of the first RHIC runs; such differences from the full detector are noted below in the description of the various analysis.

2. Charged-particle multiplicity

Global Variables such as charged-particle multiplicity characterize the events. In general, these variables are useful for determining information about the initial conditions of the collision. PHENIX has measured the charged-particle multiplicity distribution at midrapidity in Au-Au collisions at a center-of-mass energy of 130 GeV. Details of the analysis of the 130 GeV data can be found in [4] and are outlined below. The analysis of the 130 GeV data uses three PHENIX subsystems: two layers of the pad chambers (PC1 and PC3), the zero degree calorimeters, and the beam-beam counters. The PCs give three-dimensional space points along the trajectory of the charged particles and are used to provide the multiplicity measurements. The ZDC and the BBC are used in both online and offline event selection.

The primary interaction trigger requires a coincidence between firings of the two BBC. A firing is defined as having a minimum of two photomultipliers fired in one BBC. There is also a requirement that the collision vertex position is within 20 cm of $z = 0$. This trigger is based on simulations of the BBC and selects $92 \pm 2\%$ of the 7.2 b nuclear interaction cross section. (The error is systematic.)

A sample of 137,784 events was used in this analysis. All hits in PC 1 and PC3 are combined in pairs. The lines connecting the two points are projected on a plane that contains the beamline and is perpendicular to the axis of symmetry of the pad chamber system. For events with more than about 5 tracks, this produces a distinct peak that defines the vertex. Once the vertex position is known, the projection of the PC1-PC3 segment to the plane described above is compared to the measured vertex position and the difference between them, R , is plotted. The combinatorial background is removed using a mixed-event technique. Tracks up to $R = 25$ cm are counted as charged particles, a cutoff that includes 95.9% of all tracks.

Additional corrections are made for inactive areas of the chambers and electronics, the PC hit efficiency, track losses from double hit resolution, and uncounted charged tracks. The net effect of these uncertainties is a total systematic error of 6.5% at the highest multiplicities.

Events were selected which had a reconstructed vertex position within 17 cm of $z = 0$. The resulting minimum-bias charged-particle multiplicity distribution into the track acceptance $|\eta| < 0.34, \delta\phi = 88.4\text{ deg}$ is shown in Fig. 2. The distributions for the top four centrality classes (0%–5%, 5%–10%, 10%–15%, and 15%–20%) of the total interaction cross section are also shown. Centrality classes were determined by selecting events from a plot of BBC *vs* ZDC. There is an ambiguity in this distribution because the ZDC can produce a low response for both very central collisions and no collisions. This can be resolved by considering the response of a third detector. A Glauber model calculation is used to relate the centrality classes to the number of nucleons participating in the collision (N_p) and the number of binary collisions (N_c). Fig. 3 shows our results for $dN_{\text{ch}}/d\eta$ as a function of N_p . In addition, UA5 data for $p\bar{p}$ collisions at the same \sqrt{s} are shown [22]. If we extrapolate the PHENIX data to lower N_p , the result is close to the $p\bar{p}$ data.

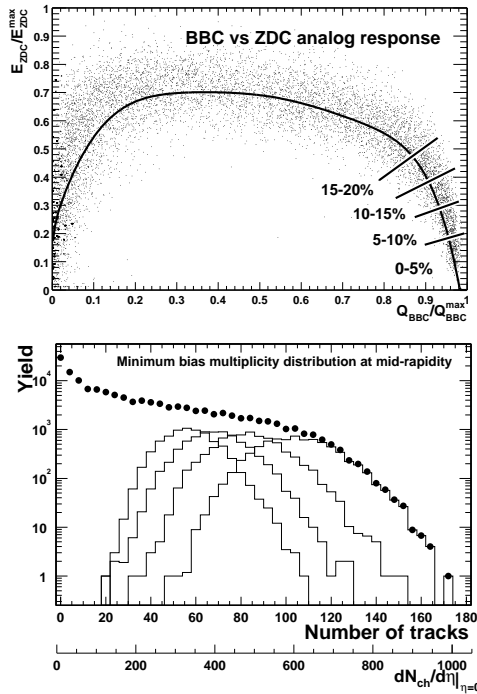


Fig. 2. BBC *vs* ZDC analog response (top panel) and minimum-bias multiplicity in the PHENIX measurement aperture (lower panel). The lower axis converts the observed distribution to the corresponding average $dN_{\text{ch}}/d\eta$ for track multiplicities less than ~ 120 ; beyond that value the shape of the distribution has a significant contribution from fluctuations into the measurement aperture. From [4].

Calculations for two collision models, HIJING [14] and EKRT [13], are also shown in Fig. 3. HIJING shows the same trend as the data, although the values are $\sim 15\%$ lower. The shape of the EKRT curve is considerably different. HIJING predicts that there are components of particle production from both soft and hard processes. Soft processes are expected to scale with N_p and hard processes with N_c . Thus we fit the data to a function:

$$dN_{\text{ch}}/d\eta = AN_p + BN_c.$$

The parameters of this fit are given in Fig. 3. The values suggest that hard processes contribute significantly to particle production. On the other hand, EKRT predicts that the gluon density is saturated by a large production of gluons. Entropy production is thus limited by gluon fusion, leading to a reduction of particle production. The PHENIX data show no evidence for such saturation effects.

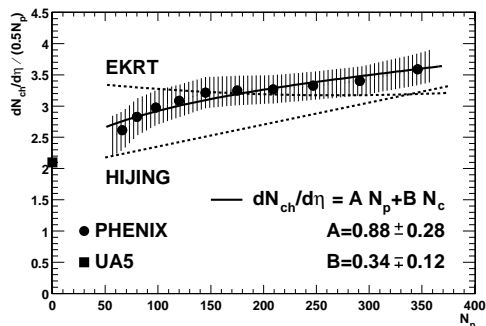


Fig. 3. Charged-particle pseudorapidity density per participant pair *vs* the number of participants. Predictions from HIJING and EKRT models and a simple phenomenological fit are also shown. The shaded area represents the systematic areas of $dN_{\text{ch}}/d\eta$ and N_p . This figure and the errors of N_c may be found in [4].

3. Hadrons at high transverse momentum

In pp collisions, the dominant source of high transverse momentum (p_T) hadrons is jet fragmentation, where the jets are the result of hard scatterings between partons [5]. Typical p_T values for such interactions are ≥ 2 GeV/ c . In high-energy heavy ion collisions, hard scattering is expected to take place early in the collision, most likely long before any formation of the quark-gluon plasma. Thus the possibility exists for the scattered partons to interact in the system, losing energy through processes such as gluon bremsstrahlung [6]. This would have the effect of reducing jet production.

Such ‘jet quenching’ would lead to a diminished yield of high p_T hadrons, an effect readily measurable on the laboratory [7,8]. If the energy loss in a QGP is greater than in hot hadronic matter, as has been suggested in [1], this observable could prove valuable as a potential signature for the formation of the QGP.

In order to determine whether the data indicate this effect is present, it is reasonable to compare the results for $A + A$ collisions to that expected in a simple binary scaling from independent nucleon–nucleon ($N + N$) collisions:

$$R_{AA}(p_T) = \frac{(1/N_{\text{evt}})d^2 N^{A+A}/dp_T d\eta}{(\langle N_{\text{binary}} \rangle / \sigma_{\text{inel}}^{N+N}) d^2 \sigma^{N+N}/dp_T d\eta}.$$

This ratio will be unity if there are no nuclear modifications to hard scattering processes. A deviation suggests the existence of nuclear medium effects. One example of a medium effect is the Cronin effect, seen in $p + A$ collisions, in which particle production for p_T above 2 GeV/ c is enhanced relative to binary scaling [9]. Another is parton shadowing [10,11], observed in lepton + nucleus collisions. Both of these effects are likely to be present in $A + A$ collisions as well as possible effects of jet quenching.

The data were taken with both of the central spectrometer arms, each having an acceptance of $\Delta\phi = 90$ deg and $|\eta| < 0.35$. The analysis is described in detail in [12]. Charged particles are reconstructed using the DC and PC systems. The momentum resolution for this configuration is $\delta p/p \sim 0.6 \cdot \otimes 3.6 p$ GeV/ c . Background to signal is negligible below a p_T of 2 GeV/ c , 1/10 for 3.5 GeV/ c , and 1/1 for a p_T of 6 GeV/ c . A full GEANT simulation is used to correct the data for acceptance, reconstruction efficiency, in-flight decays, momentum resolution, and dead regions. Track reconstruction efficiency ranges from 98 % for peripheral collisions, to $68 \pm 6\%$ for central collisions.

The decay $\pi^0 \rightarrow \gamma\gamma$ is used to observe neutral pions. Two methods are used to detect photons — a lead-scintillator sampling calorimeter and a lead-glass Cerenkov calorimeter. Hadron showers are suppressed using cuts on shower shape and arrival time. The combinatorial background for the pair data is subtracted using a mixed-event analysis. The data are also corrected for energy resolution, overlapping clusters, analysis cuts, dead regions of the detectors, and acceptance. Results from both detectors are in good agreement. There is a contamination from pions not originating at the vertex which is estimated to be 6%–8%.

The event classification is similar to that described above for the multiplicity data. The central data sample includes the 10% most central fraction of the geometrical cross section. The peripheral sample contains events in the 60%–80% centrality bin. Using a Glauber model, we calculate that this

corresponds to $\langle N_{\text{binary}} \rangle = 905 \pm 96$ for events in the central sample, and $\langle N_{\text{events}} \rangle = 20 \pm 6$ in the peripheral sample. Fig. 4 shows the p_T distributions for charged hadrons and neutral pions for both central and peripheral events as described above, along with the yields estimated assuming binary scaling. For the peripheral data, both charged and neutral, the binary-scaling estimate agrees well with the data above a p_T of 2 GeV/ c . The central data lies below the binary-scaling calculation, with the difference being especially pronounced for the π^0 's.

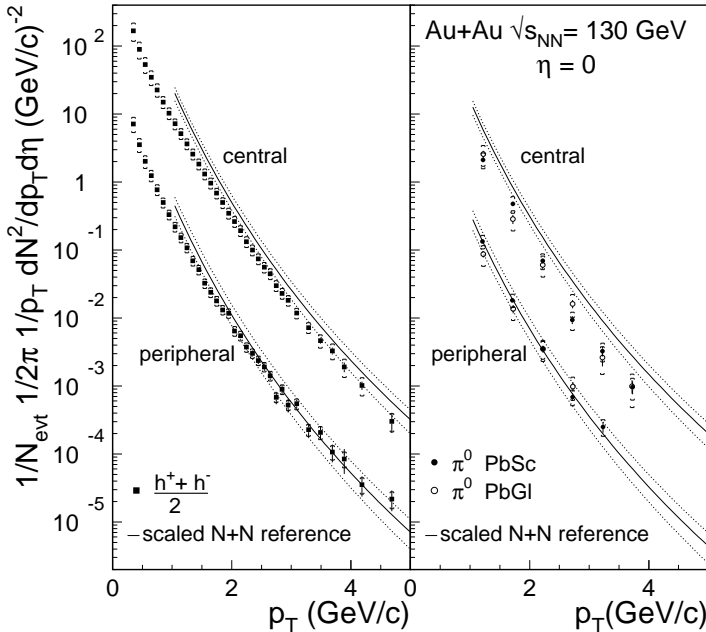


Fig. 4. The yields per event at mid-rapidity for charged hadrons (left) and neutral pions (right) are shown as a function of p_T for 60%–80% (lower) and 0%–10% (upper) event samples. The error bars indicate the statistical errors on the yield; the surrounding brackets indicate the systematic errors. Also shown are the $N + N$ references for charged hadrons and neutral pions, each scaled up by $\langle N_{\text{binary}} \rangle$ for the class. The bands indicate the uncertainty in the $N + N$ reference and in $\langle N_{\text{binary}} \rangle$. (Figure from [12].)

Fig. 5 shows a plot of R_{AA} as a function of transverse momentum. Above 2 GeV/ c , R_{AA} lies well below unity for both the charged hadron and neutral pion spectra. This is to be compared to the expectation that the Cronin effect will enhance the production of high p_T particles (> 2 GeV/ c). For comparison, the plot also shows the ratio of the inclusive particle production of $\alpha + \alpha$ to that of $p + p$ at $\sqrt{s_{NN}} = 31$ GeV and from $A + A$ compared to $p + p$ collisions at $\sqrt{s_{NN}} = 17$ GeV. Both of these results show $R > 1$ for

$p_T > 2\text{GeV}$. The suppression at high- p_T for Au+Au collisions at $\sqrt{s_{NN}} = 130\text{ GeV}$ is suggestive of the model of energy loss by scattered partons by a dense medium. However, it is necessary to eliminate other possible nuclear medium effects before a definitive interpretation can be made. A series of measurements in $p + A$ collisions at RHIC are planned which should make the picture clearer.

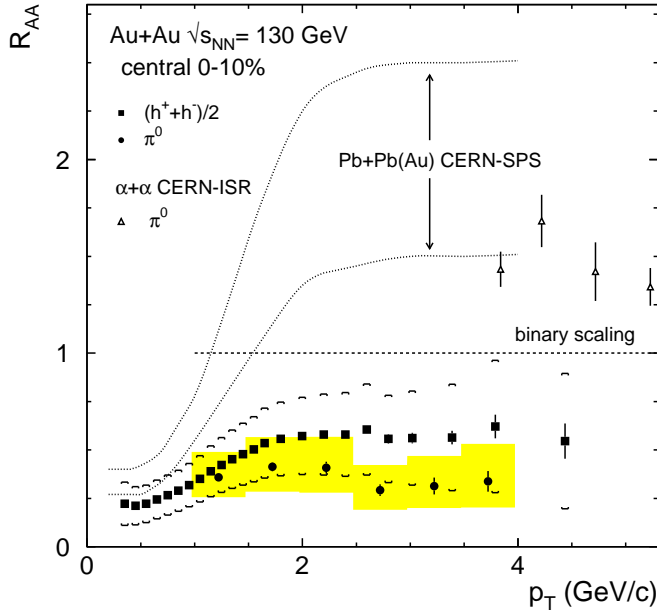


Fig. 5. The ratio R_{AA} for charged hadrons and neutral pions (weighted average of PbGl and PbSc results) in central Au+Au collisions. The error bars represent the statistical error on the measurement. The surrounding bands [shaded for π^0 s, brackets for $\frac{h^+ + h^-}{2}$] are the quadrature sums of (i) the systematic errors on the measurement (ii) the uncertainty in the $N + N$ reference, and (iii) the uncertainty in $\langle N_{\text{binary}} \rangle$. Also shown are the ratio of inclusive cross sections in $\alpha + \alpha$ compared to $p + p$ at $\sqrt{s_{NN}} = 31\text{GeV}$ [15], and spectra from central Pb + Pb, Pb+Au compared to $p + p$ collisions at $\sqrt{s_{NN}} = 17\text{GeV}$ [16] shown as a band indicating the range of uncertainty. (Figure from [12].)

4. Single electron spectra and open charm production

The production of heavy quarks in relativistic heavy ion collisions can be a useful probe of the hot, dense matter resulting from the collisions. We have used single electron spectra to study heavy quark production at RHIC. Besides being sensitive to the initial state gluon density [18,19], charm measurements will be needed to understand J/Ψ suppression [20,21].

We analyzed 1.23 M minimum bias events with a vertex selection $|z| < 30$ cm. Only the west arm of the central spectrometer is used. (Details of the analysis are given in [17].) The DC and PC1 are used to reconstruct charged particle tracks with a momentum resolution given above. A confirming hit in the EMCAL is required. The resolution of the EMCAL is $8.2\%/\sqrt{E\text{GeV}} \otimes 1.9\%$. The EMCAL and the RICH are used for electron identification and appropriate quality cuts are applied to the RICH hit pattern and the E/p ratio. Combinatorial background is subtracted using event-mixing. The electron acceptance is $\sim 7.4\%$ of dN/dy and the efficiency is $\sim 60\%$; both are determined by a GEANT simulation. There is a loss in efficiency that is dependent on centrality but independent of p_T ; the efficiency is $27 \pm 4\%$ for central collisions and $4 \pm 2\%$ for peripheral collisions.

The electron p_T spectra for peripheral, minimum-bias, and central collisions is shown in Fig. 6. The error bars are statistical, while the systematic error is about 11%. These spectra contain background from (i) Dalitz decays of π^0 , η , η' , ω , and ϕ , (ii) dielectron decays of ρ , ω , and ϕ , (iii) photon conversions, (iv) kaon decays. Signal electrons come from (i) semileptonic charm decay, and (ii) bottom decays and thermal dileptons. The sources of background are estimated using a hadron event generator as input to a GEANT simulation.

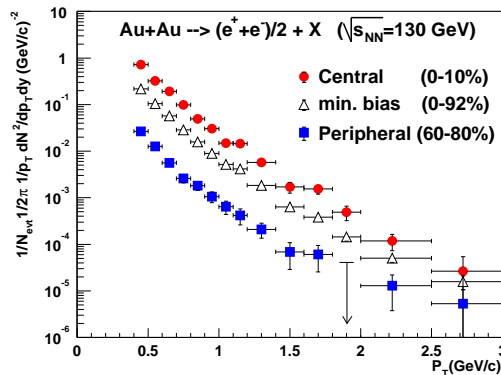


Fig. 6. Transverse momentum spectra of electrons in PHENIX from Au + Au collisions at $\sqrt{s_{NN}} = 130$ GeV. (Figure from [17].)

The bottom panel of Fig. 7 gives the relative contributions to the background from the various sources. The major source of background is from π^0 decays from both Dalitz decay and photon conversions. The next most significant source is η decays. The π^0 spectrum is constrained by our measurements while an estimate of the η/π ratio indicates that the η background estimate is conservative. Background from the decays of all other hadrons

contribute only a few percent to the total. The upper panel of Fig. 7 shows the ratio of the measured electron spectrum to the calculated background as a function of p_T for minimum bias events. The shaded region indicates the envelope of the estimate of the systematic errors. There is a definite excess of electrons above the background for $p_T > 0.6$ GeV/ c . The plot for central collisions is similar, while the peripheral data has insufficient statistics.

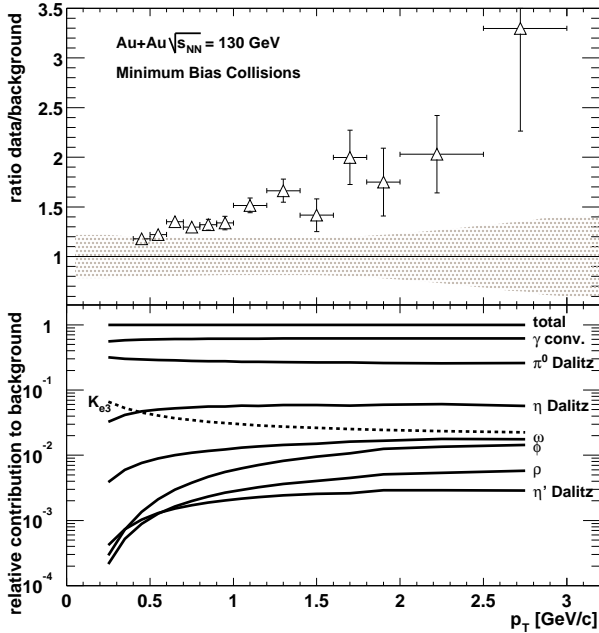


Fig. 7. Ratio of the electron data to the calculated background as a function of p_T in minimum bias collisions (upper panel) and relative contributions to the background from various sources (lower panel). The curves for ω and ϕ show the sum of the Dalitz and the dielectron decay modes. (Figure from [17].)

Fig. 8 shows the background-subtracted electron spectra for minimum-bias (0%–92%) and central (0%–10%). Also shown are the results of a PYTHIA calculation of electron spectra from charm decay convolved with a nuclear overlap integral calculated from a Glauber model. The calculated spectra agree reasonably well with the data. PHENIX data taken at higher energy ($\sqrt{s_{NN}} = 200$ GeV/ c) with a larger data sample is now available and should allow us to better understand heavy-quark production in Au + Au collisions at RHIC.

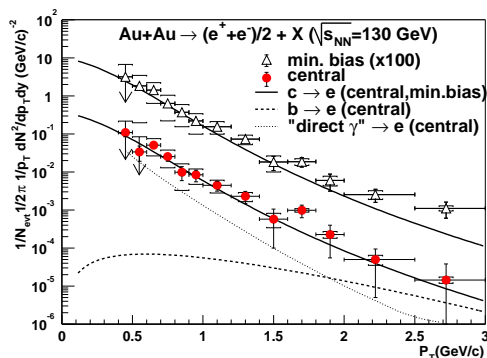


Fig. 8. The background-subtracted electron spectra for minimum-bias (0%–92%) (scaled up by a factor of 100) and central(0%–10%) collisions compared with the expected contributions from open charm decays. Also shown, for central collisions only, are the expected contribution from bottom decays (dashed line) and the conversion electron spectrum from a direct photon prediction (dotted line). (Figure from [17].)

5. Conclusions

Here I have presented a few of the early results from the PHENIX detector at RHIC. We have examined the charged particle multiplicity and used the results to evaluate two different collision models, HIJING and EKRT. We have observed the suppression of hadrons at large transverse energy, an interesting result that agrees qualitatively with a model of energy loss by scattered partons in a dense medium. Finally, we have found that the electron spectra, after subtraction of background decays, is consistent with arising from charm decay. We look forward to analyzing data from PHENIX at the full RHIC energy to continue to expand our understanding of the hot, dense matter produced in high-energy heavy ion collisions.

REFERENCES

- [1] R. Baier, D. Schiff, B.G. Zakharov, *Ann. Rev. Nucl. Part. Sci.* **50**, 37 (2000).
- [2] K. Ikematsu *et al.*, *Nucl. Instrum. Methods Phys. Res.* **A411**, 238 (1998).
- [3] C. Adler *et al.*, *Nucl. Instrum. Methods Phys. Res.* **A470**, 488 (2001).
- [4] K. Adcox *et al.*, [PHENIX Collaboration] *Phys. Rev. Lett.* **86**, 3500 (2001).
- [5] J.F. Owens, E. Reya, M. Gluck, *Phys. Rev.* **D18**, (1978).
- [6] M. Gyulassy, M. Plumer, *Phys. Lett.* **B243**, 432 (1990).
- [7] Xin-Nian Wang, M. Gyulassy, *Phys. Rev. Lett.* **68**, 1480 (1992).

- [8] Xin-Nian Wang, *Phys. Rev.* **C58**, 2321 (1998).
- [9] D. Antreasyan *et al.*, *Phys. Rev.* **D19**, 764 (1979).
- [10] J.J. Aubert *et al.*, [European Muon Collaboration] *Phys. Lett.* **B123**, 275 (1983).
- [11] R.G. Arnold *et al.*, *Phys. Rev. Lett.* **52**, 727 (1984).
- [12] K. Adcox *et al.*, [PHENIX Collaboration] *Phys. Rev. Lett.* **88**, 022301 (2002).
- [13] K.J. Eskola, K. Kajantie, P.V. Ruuskanen, K. Tuominen, *Nucl. Phys.* **B570**, 379 (2000).
- [14] Xin-Nian Wang, M. Gyulassy, *Phys. Rev.* **D44**, 3501 (1991).
- [15] A.L.S. Angelis *et al.*, [BCMOR Collaboration] *Phys. Lett.* **B185**, 213 (1987).
- [16] Enke Wang, Xin-Nian Wang, *Phys. Rev.* **C64**, 034901 (2001).
- [17] K. Adcox, *et al.*, [PHENIX Collaboration], *Phys. Rev. Lett.* **88**, 192303 (2002).
- [18] J.A. Appel, *Ann. Rev. Nucl. Part. Sci.*, **42**, 367 (1992).
- [19] B. Muller, Wang, Xin-Nian, *Phys. Rev. Lett.* **68**, 2437 (1992).
- [20] T. Matsui, H. Satz, *Phys. Lett.* **B178**, 416 (1986).
- [21] M.C. Abreu *et al.*, [NA50 Collaboration], *Phys. Lett.* **B477**, 28 (2000).
- [22] G.J. Alner *et al.*, [UA5 Collaboration], *Z. Phys.* **C33**, 1 (1986).